Expanded View Figures

Figure EV1. MATR3 modulates redistribution of chromatin in nuclei.

A Immuno-electron microscopy analysis of MATR3 protein distribution labeled by DAB in the AML12 cell. The solid arrows point to the individual DAB signal and the hallow arrows point to the clustered DAB signals, both of which represent MATR3 proteins. NM, nuclear membrane; Nu, nucleolus. Scale bars, (i): 2 μm; (ii): 0.5 μm; (iii), (iv): 0.2 μm.

B (Upper) Super-resolution fluorescence microscopy images showing relative distribution between MATR3 and histone modifications (H3K9me3, H3K9me2, H3K27me3, H3K27ac and H3K4me3) in AML12 cells. (Lower) Line charts showing pixel intensity of each channel on the regions of interest (ROI). *r*, coefficient of correlation. Scale bars, 5 μm.

C (Left) Representative cross-section images showing nuclear localization of MATR3 and H3K27me3 upon Ctrl, MATR3 knockdown (+Dox) and MATR3 rescue (±Dox). (Right) Line charts showing pixel intensity of each channel on the ROIs. Scale bars, 10 μm.

D Pixel intensity of ROIs showing relative distribution of H3K27me3 and Lamin A/C upon Ctrl, MATR3 knockdown (+Dox) and MATR3 rescue (±Dox). L_0, region between nuclear membrane. L_1, region between two H3K27me3 pixel peaks that closest to the nuclear membrane. Scale bars, 5 μm.

E Pixel intensity of ROIs showing relative distribution of H3K27me3 and C23. N_0, region between nucleolus membrane (position of nucleolus membrane on X-axis determined by C23 pixel half-peaks on both sides). N_1, region between two H3K27me3 pixel peaks that closest to the nucleolus membrane. Scale bars, 5 μm.

F Standard deviation of H3K27me3 pixel intensity of Ctrl (n = 98), MATR3 knockdown (+Dox) (n = 100) and MATR3 rescue (±Dox) (n = 94). The *P*-values were calculated using unpaired two-tailed Student's *t*-test; *$P < 0.05$, ****$P < 0.0001$. Error bars indicate mean ± s.e.m.

G Genome browser of the H3K27me3 enriched region in Ctrl and MATR3 knockdown (+Dox) samples.

H Immunofluorescent detection of the efficiency of MATR3 knockdown in ES cells after 6 h addiction of 500 μM IAA or equal volume of alcohol (−IAA). Scale bars, 10 μm.

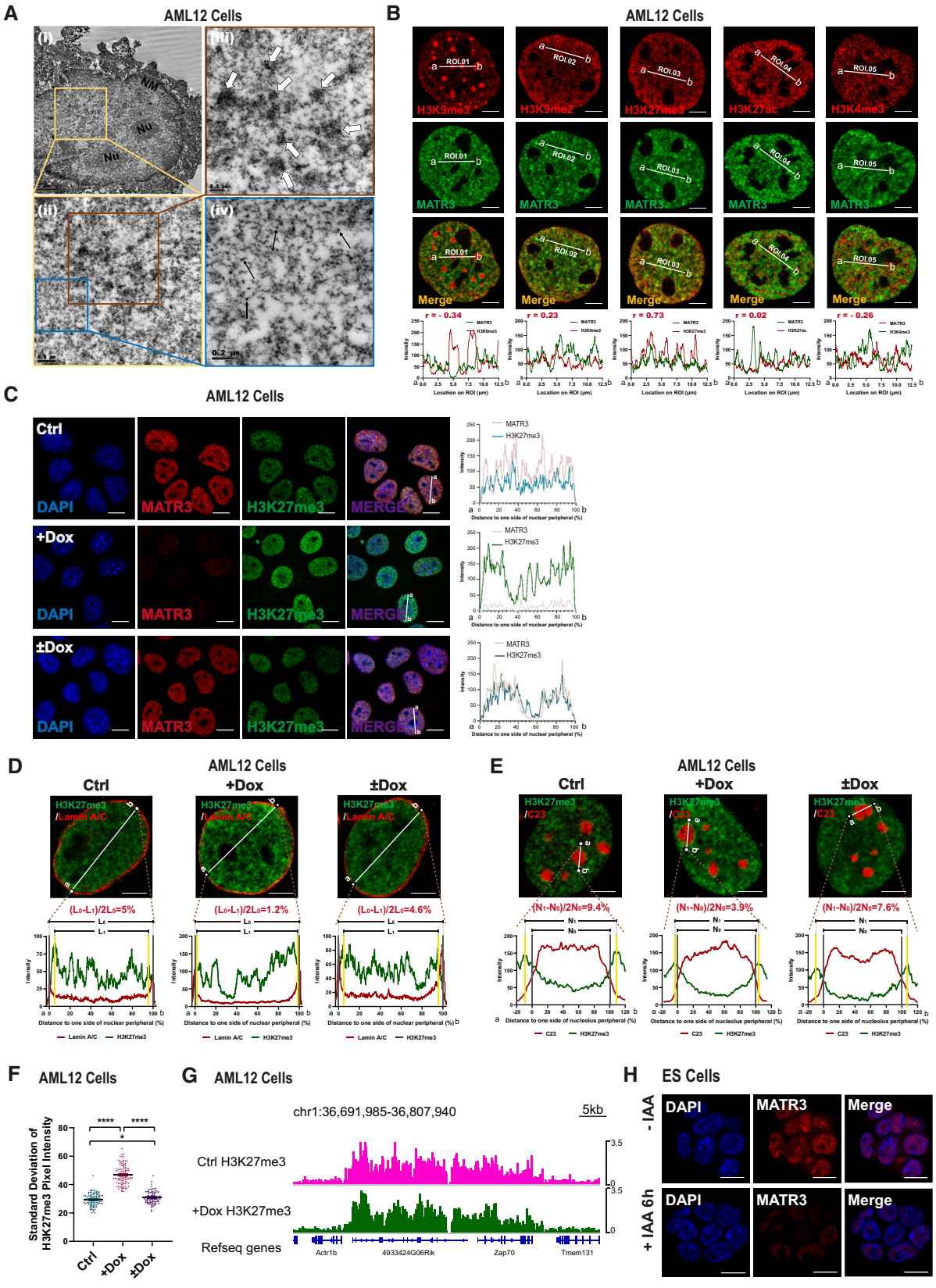

Figure EV1.

Figure EV2. MATR3 associates with antisense L1 RNAs.

A Representative cross-section images showing distribution pattern for MATR3 in cell nuclei after 0, 1, 2, 6, 12, 24 h treating with 75 μM DRB. Scale bars, 10 μm.

B Statistics for MATR3 distribution pattern in cell nuclei after 0 (n = 500), 1 (n = 578), 2 (n = 560), 6 (n = 495), 12 (n = 489), 24 (n = 490) hours treating with 75 μM DRB.

C Heatmap of MATR3 RIP-seq sense and antisense mean reads count in repetitive elements in ES cells. All RE copies with the RIP (MATR3 -IgG) count number ≥ 10 are kept. For each RE family, RE copies from antisense and sense of two replicates are merged. Then, compute the RIP (MATR3 -IgG) count number for RE copies and compute the mean count of RIP (MATR3 -IgG) of each sample.

D Genomic distribution of MATR3-AS L1 RNAs loci in AML12 cells.

E **(**Left) Genome browser of the MATR3 RIP, RepeatMasker and Refseq genes. Targeting loci of the primers were noted on the screenshot. (Right) DNA gel images of RT–PCR of MATR3 RIP products (and input RNAs).

F Scatter plot of RIP-seq antisense for MATR3-associated L1 copies (AS L1) and host genes' expression. ASL1 copies that with RIP (MATR3 -IgG) count number ≥ 10 and located within gene body regions are kept. *X*-axis: RIP (MATR3 -IgG) count of ASL1 copies. *Y*-axis: the FPKM of ASL1's host genes as detected by RNA-seq. Pearson correlation coefficient (PCC) between RIP (MATR3 -IgG) count number of ASL1 copies and FPKM of host genes.

G RNA decay curve for AS L1 RNAs, Neat1 RNA and Actb RNA after blocking transcription with 5 μg/ml actinomycin D before and after MATR3 depletion. RNA remaining was measured relative to 18 s RNA at 0 h by qPCR. The RNA decay assay was performed in three independent biological replicates (N = 3). Fit modeled by one-phase decay using nonlinear least squares regression. Error bars indicate mean ± s.d.

H (Left) Representative cross-section images showing relative distribution between AS L1 RNA with MATR3 in ES cells. (Right) Line charts showing pixel intensity of each channel on the ROIs. Scale bars, 5 μm.

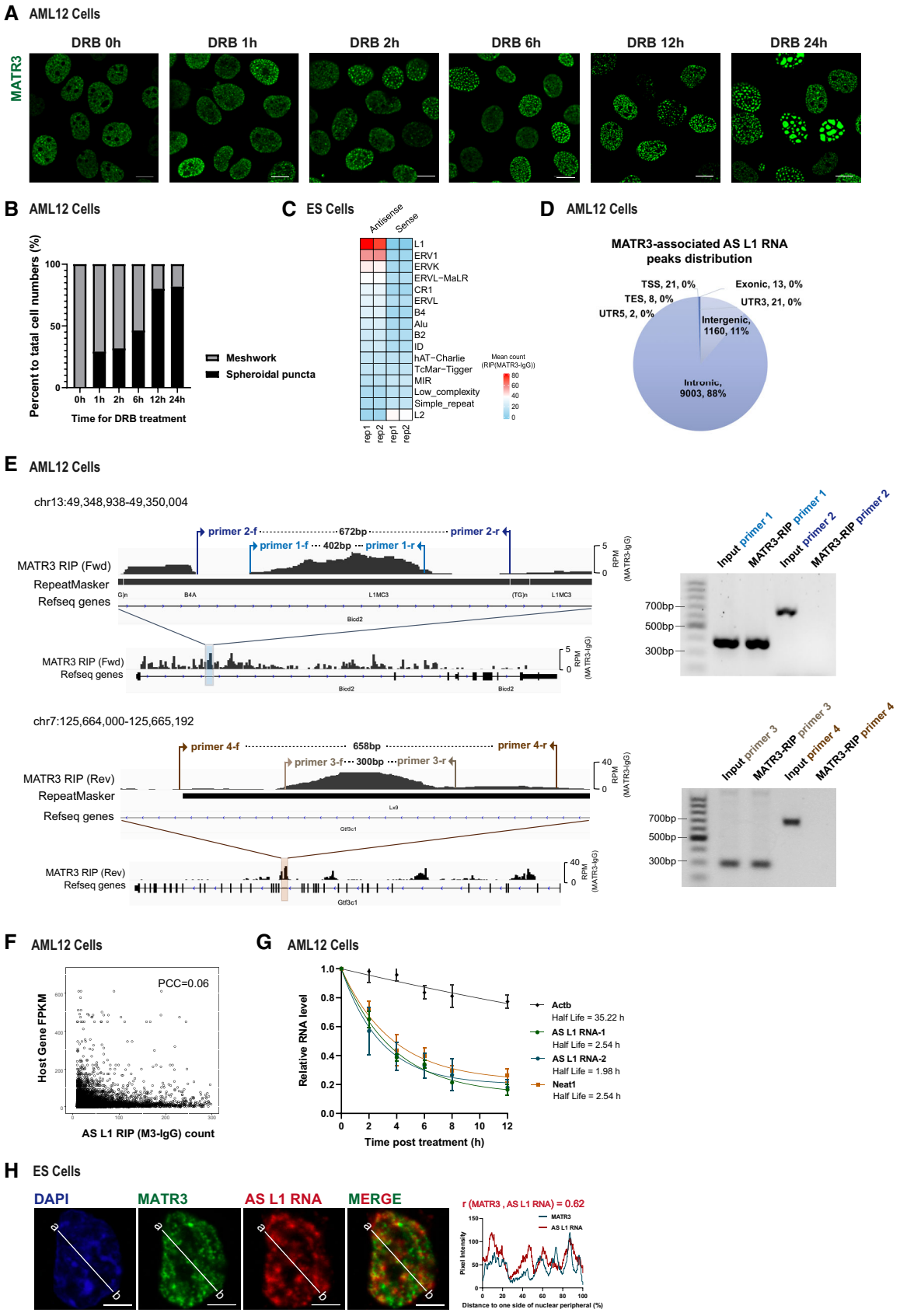

Figure EV2.

Figure EV3. AS L1 RNAs depletion affects nuclear distribution of MATR3.

A Representative RNA FISH (with probes targeting antisense L1_Mus1 RNAs) and immunofluorescence images showing nuclear distribution of AS L1 RNAs and MATR3 after 24 h treating with different ASOs in AML12 cells. Scales bars, 10 μm.

B Statistical data for intracellular distribution of MATR3 proteins after 24 h treating with Scramble (n = 200), antisense L1_Mus1 (n = 198), sense L1_Mus1 (n = 195), antisense L1_MA7 (n = 200) and sense L1_MA7 (n = 200) in AML12 cells.

C The representative intracellular distribution of MATR3 proteins before and after treating with AS L1 ASOs in AML12 cells. Scales bars, 5 μm.

D Statistical data for intracellular distribution of MATR3 proteins after 0 h (n = 1,000), 6 h (n = 1,280), 12 h (n = 1,504) and 24 h (n = 1,430) treating with AS L1 ASOs in AML12 cells.

E, F The representative cross-section image showing nuclear distribution of MATR3 and HNRNPU (E) and SAFB (F) before and after 24 h treating with antisense L1 ASOs in AML12 cells. Scales bars, 5 μm.

G (Left) The representative cross-section image showing nuclear distribution of MATR3 and FUS before and after 24 h treating with antisense L1 ASOs in AML12 cells. (Right) The zoom-in MERGE image showing relative distribution of MATR3 and FUS. Line charts showing pixel intensity of each channel on the ROIs. Scales bars, 5 μm.

H Scatter plot of antisense RNA expression changes in L1_Mus1 subfamily with genes expression of host between AS L1 ASO and scramble ASO treatment samples. Mus1 copies located within gene body regions are kept. *X*-axis: antisense RNA expression fold changes $\log_2$(AS L1 ASO/scramble ASO) of Mus1 copies. *Y*-axis: the FPKM fold changes in L1_Mus1's host genes. Pearson correlation coefficient (PCC) between antisense RNA expression changes in Mus1 copies and expression changes in host genes.

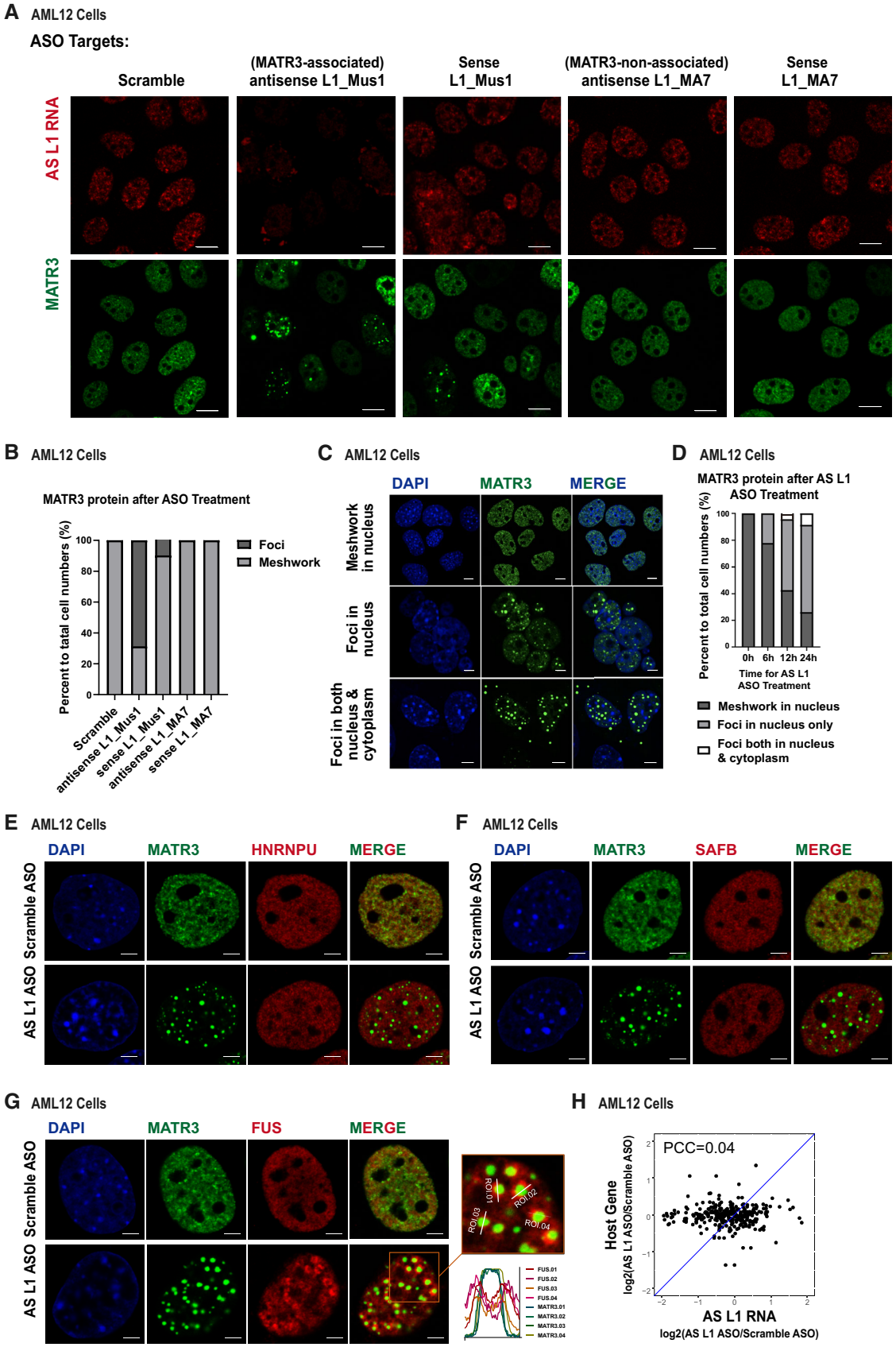

Figure EV3.

Figure EV4. 3D genome organization as revealed by Hi-C with ES cells.

A Venn diagram shows the common and sample-specific TADs between Ctrl and MATR3-AID samples from ES cells. The TADs that overlapped length/TAD length > 0.8 both in Ctrl and MATR3-AID samples were identified as common TADs.

B Intra-TAD contacts changes in MATR3-AS L1 RNAs associated and nonassociated TADs from ESC cells. For each TAD, we calculate the density of the anti-MATR3 RIP-seq signal of AS L1 RNAs. TADs are grouped into "No AS L1" and "with AS L1" by density greater than 0 or not. The number of TADs associated with MATR3-AS L1 RNAs and nonassociated are 2001 and 639. The box of the boxplot covers the 50% of the values between 1st quartile and 3rd quartile of each group; Boxplot whiskers represent the minimal and maximal values of each group; The horizontal line of box represents the median value of each group; Red dashed lines indicate the zero.

C Intra-TAD contacts changes in TADs nonassociated with MATR3-AS L1 RNAs and four quantile groups associated with MATR3-AS L1 RNAs ranking by increasing in MATR3-AS L1 RNAs density from ES cells. The number of TADs nonassociated with MATR3-AS L1 RNAs and associated four quantile groups is 639, 500, 500, 500 and 501. The box of the boxplot covers the 50% of the values between 1st quartile and 3rd quartile of each group; Boxplot whiskers represent the minimal and maximal values of each group; The horizontal line of box represents the median value of each group; Red dashed lines indicate the zero.

D Percentage of TADs located in compartments A or B regions from five TAD groups (same groups in C) from ES cells.

E Insulation strength at TAD boundaries within compartment A, B regions or at AB boundaries of Ctrl and MATR3-AID from ES cells.

F Percentages of compartment status at unswitched A, unswitched B, B switched to A and A switched to B between Ctrl and MATR3-AID from ES cells.

G Changes in contacts between compartment regions from the same (AA or BB) and different (AB) type in Ctrl and MATR3-AID from ES cells. The *y*-axis showing log2 contacts changes between MATR3-AID and ctrl cells. The contacts are the density of the observed contacts normalized by the density of the expected contacts. The box of the boxplot covers the 50% of the values between 1st quartile and 3rd quartile of each group; The horizontal line of box represents the median value of each group; Red dashed lines indicate the zero.

H Changes in contacts within A or B compartment regions between Ctrl and MATR3-AID from ES cells. Data are represented as boxplots based on $\log_2$(O/E-MATR3-AID / O/E-Ctrl) values per compartment region. The number of compartment A and B are 938 and 991. The box of the boxplot covers the 50% of the values between 1st quartile and 3rd quartile of each group; Boxplot whiskers represent the minimal and maximal values of each group; The horizontal line of box represents the median value of each group; Red dashed lines indicate the zero.

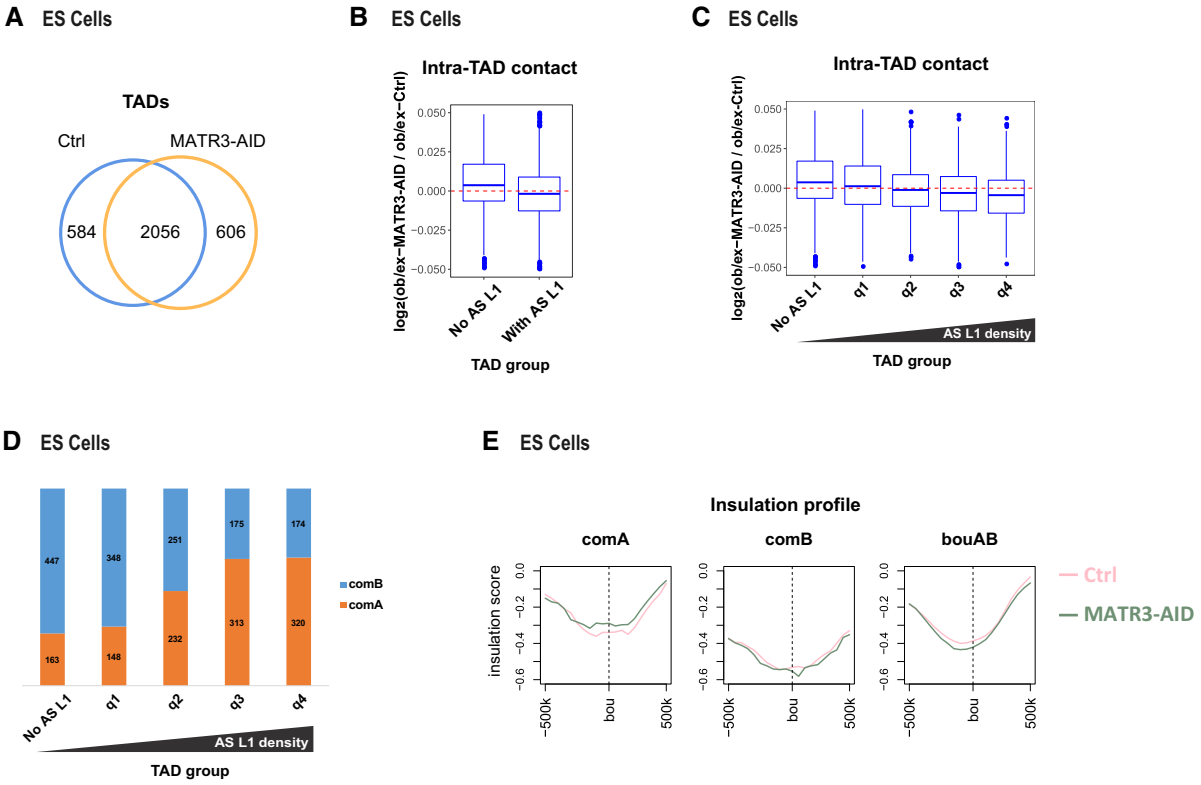

Figure EV4.

Figure EV5. MATR3 regulates the localization of PcG proteins.

A (Left) Representative cross-section images showing relative distribution between MATR3 and PcG proteins BMI-1 and EZH2. (Right) Line charts showing pixel intensity of each channel on the ROIs. r represents coefficient of correlation. Scale bar, 5 μm.

B (Upper) Western blotting of anti-MATR3 immunoprecipitation (anti-IgG IP as negative control) products hybridized with MATR3, EZH2 and BMI-1 antibodies. (Lower) Western blot of anti-EZH2 immunoprecipitation (anti-IgG IP as negative control) products hybridized with EZH2 and MATR3 antibodies.

C, D The representative cross-section image showing nuclear distribution of BMI-1 (C) and EZH2 (D) in Ctrl and shMatr3 (+Dox 3d) cells. Scale bar, 10 μm.

E (Upper) Standard deviation of BMI-1 pixel intensity upon Ctrl (n = 86) and shMatr3 (+Dox 3d) (n = 89) cells. ****$P < 0.0001$, Student's t-test. Error bars represent SD. (Lower) Standard deviation of EZH2 pixel intensity upon Ctrl (n = 86) and shMatr3 (+Dox 3d) (n = 97) cells. The P-values were calculated using unpaired two-tailed Student's t-test; ****$P < 0.0001$. Error bars indicate mean ± s.e.m.

F Western blotting showing the distribution of BMI-1 and EZH2 proteins in chromatin-non-associated and chromatin-associated extracts before and after MATR3 knockdown (+Dox 3d) in AML12 cells. Representative of two independent replicates with similar results.

G, H (Left) The representative cross-section image showing nuclear distribution of BMI-1 (G) and EZH2 (H), and colocalization with H3K27me3 upon Ctrl and MATR3 knockdown (+Dox 3d). (Right) Line charts showing pixel intensity of each channel on the ROIs. r, coefficient of correlation Scale bar, 5 μm.

I The RNA level of *Gapdh*, *Malat1*, *Neat1* and *Hnf1aos1* in anti-EZH2 RIP products relative to that in anti-IgG RIP products as detected by RT–qPCR. For each sample, the relative RNA level was normalized to *Actb*. The RIP–qPCR assay was performed in six independent biological replicates (n = 6). The P-values were calculated using unpaired two-tailed Student's t-test; ns, not significant. Error bars indicate mean ± s.d.

J (Upper) Western blotting showing the protein level of MATR3 and BMI-1 in shCtrl and shBmi-1 cells; (Lower) Western blotting showing the protein level of MATR3 and EZH2 in shCtrl and shEzh2 cells.

K The representative images showing nuclear colocalization of MATR3 with AS L1 RNA in shCtrl, shBMI-1 and shEZH2 AML12 cells. Scales bar, 5 μm.

L Coefficient of correlation between MATR3 and AS L1 RNA in shCtrl (n = 42), shBMI-1 (n = 48) and shEZH2 (n = 46) AML12 cells. The P-values were calculated using unpaired two-tailed Student's t-test; ns, not significant. Error bars indicate mean ± s.e.m.

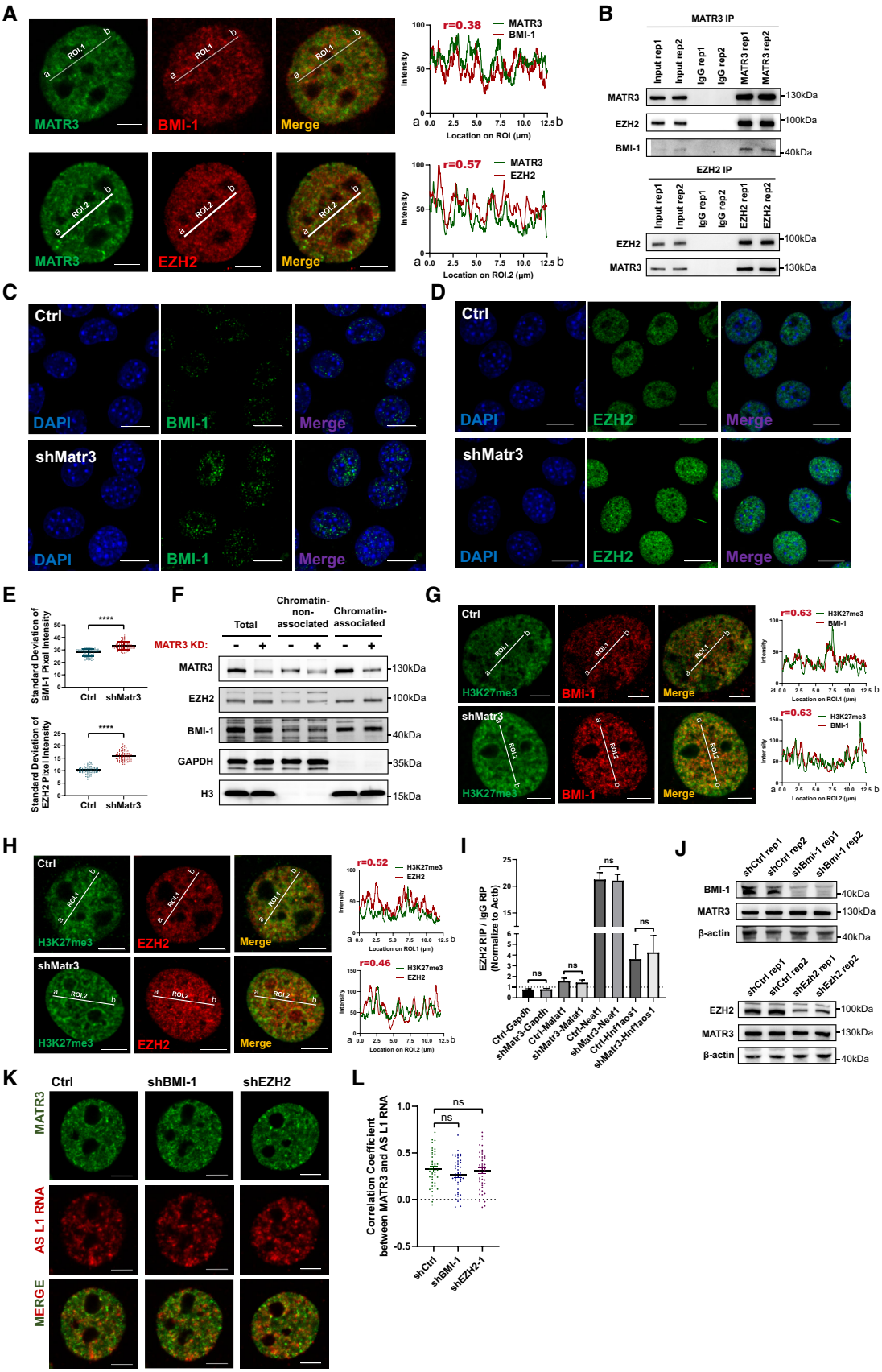

Figure EV5.